Interference effects in L-shell atomic double photoionization

A. S. Kheifets†
RSPE, The Australian National University, Canberra ACT 0200, Australia

I. Bray
Institute of Theoretical Physics, Curtin University, WA 6845 Perth, Australia

J. Colgan
Theoretical Division, Los Alamos National Laboratory, Los Alamos, NM 87545

M. S. Pindzola
Department of Physics, Auburn University, Auburn, AL 36849, USA

Abstract. Angular correlation pattern in two-electron continuum is very similar in double photoionization (DPI) of a neutral atom $\gamma + A \to A^{2+} + 2e^-$ and electron-impact ionization of the corresponding singly charged ion $e^- + A^+ \to A^{2+} + 2e^-$. This allows us to identify and to interpret interference effects in DPI of various L-shell atomic targets such as the metastable He* $1s2s\,^1S$ and the ground state Li $1s^2 2s$ and Be $1s^2 2s^2$.

PACS numbers: 32.30.Rj, 32.70.-n, 32.80.Fb, 31.15.ve

† Corresponding author: A.Kheifets(at)anu.edu.au

Double photoionization (DPI) of an atom or a molecule by a single photon is a process driven by many-electron correlation. Due to well defined angular momentum and spin of the probe (photon), the most essential many-electron dynamics of the DPI process can be separated from the trivial kinematic factors. This dynamics is contained in a pair of the symmetric *gerade* (g) and antisymmetric *ungerade* (u) DPI amplitudes. The latter amplitude is vanishing in the special case of equal energy sharing between the photoelectrons. In this case, the fully-resolved triply-differential cross-section (TDCS) of DPI can be written as

$$\frac{d^3\sigma_{(\gamma,2e)}}{d\Omega_1 d\Omega_2\, dE_2} = \Big|[\boldsymbol{e}\cdot\boldsymbol{n}_1 + \ \boldsymbol{e}\cdot\boldsymbol{n}_2]\ \mathcal{M}^g(\theta_{12})\Big|^2 \ . \tag{1}$$

Here the unit vectors $\boldsymbol{n}_1$, $\boldsymbol{n}_2$ and $\boldsymbol{e}$ denote escape directions of the photoelectrons and the polarization vector of light, respectively. A more general expression with an arbitrary spin of the target and unequal energy sharing between photoelectrons is given in our earlier paper (Kheifets *et al* 2010).

Following the pioneering work by Schwarzkopf *et al* (1993) on DPI of He, it is customary to describe the symmetric amplitude by a Gaussian ansatz

$$\Big|\mathcal{M}^g(\theta_{12})\Big| \approx A\exp\left[-2\ln 2\left(\frac{\pi-\theta_{12}}{\Delta\theta}\right)^2\right] \ . \tag{2}$$

The full width at half maximum parameter $\Delta\theta$ depends on the energy of the photon as prescribed by the Wannier theory (Huetz *et al* 1991). It also depends on the target orbital being ionized. Kheifets & Bray (2006) demonstrated that, at the same photon energy, DPI of a more sparse electron shell produces a tighter Gaussian and vice versa. This can be interpreted in terms of the number of partial waves in the photoelectron wave function reaching the target orbital. Due to a centrifugal barrier, a short range radial orbital can be reached by fewer ℓ-partial waves in comparison with a more extended orbital. As the angular momentum ℓ and the Gaussian width $\Delta\theta$ are the conjugate variables, restriction in ℓ results in larger uncertainty in angular distribution and, consequently, a wider Gaussian.

Even though the Gaussian ansatz (2), as derived from the Wannier threshold theory, should be valid at small excess energies, it can be used as a practical tool at a much wider range of photon energies. In the case of He, the Gaussian parameterization describes the symmetric DPI amplitude quite accurately up to 80 eV excess energy (Kheifets & Bray 2000). Given this successful application, one would also hope to use the Gaussian ansatz to describe DPI in other atomic targets beyond He. Lithium is the simplest atom in this category. However, symmetric amplitudes of DPI of Li, both in the singlet and triplet channels, turned out to be strongly non-Gaussian at a fairly small excess energy of 10 eV (Kheifets *et al* 2010*a*). This was confirmed by the follow up analysis of the arbitrary energy sharing case (Kheifets *et al* 2010).

In the present work, we analyze this effect systematically in DPI of other L-shell atomic targets such as metastable He* $1s2s\,^1S$ and the ground state Be $1s^22s^2$. We find a strong deviation from the Gaussian ansatz in all these targets. In a search for clues

as to the origin of this effect, we notice that the DPI process $\gamma + A \rightarrow A^{2+} + 2e^-$ is closely related to electron impact ionization of the corresponding singly charged ion $e^- + A^+(nl) \rightarrow A^{2+} + 2e^-$. This correspondence is due to the fact that the DPI process, occurring not very far from its threshold, proceeds predominantly via the knock-out mechanism (Kheifets 2001). In this mechanism, the primary photoelectron is ionized by a direct photon absorption and the secondary photoelectron is ejected via electron impact ionization of the singly charged ion. Thus the DPI process mimics, to a large extent, the angular correlation pattern seen in electron impact ionization of the corresponding ion. To derive this pattern, we consider an (e,2e) reaction in the doubly symmetric coplanar kinematics when the two outgoing electrons are detected at equal energies and equal angles relative to the direction of the incident projectile. When the two-electron continuum is restricted to the singlet dipole ^1P state, the fully resolved TDCS of such an (e,2e) reaction can be written similarly to Equation (1) as

$$\frac{d^3\sigma_{(e,2e)}}{d\Omega_1 d\Omega_2\, dE_2} = \Big|\Big(\cos\theta_1 + \cos\theta_2\Big)\mathcal{M}^g_{(e,2e)}(\theta_{12})\Big|^2 \ , \tag{3}$$

where $\theta_{12} = \theta_1 + \theta_2$ for the kinematics under consideration. Equation (3) follows directly from the general angular dependence $\mathcal{Y}_1(\boldsymbol{n}_1, \boldsymbol{n}_2) \cdot \boldsymbol{n}_0$ of the two-electron continuum in the dipole channel. Here $\mathcal{Y}_1(\boldsymbol{n}_1, \boldsymbol{n}_2)$ is a bypolar harmonic and $\boldsymbol{n}_0$ is the direction of incidence taken as the quantization axis.

We calculate the DPI amplitudes of various homo-shell (He $1s^2$, Be $2s^2$) and hetero-shell (He* $1s2s$ and Li $1s^22s$) atomic targets using the convergent close-coupling (CCC) (Kheifets & Bray 2002, Kheifets & Bray 2001) and time-dependent close-coupling (TDCC) methods (Colgan & Pindzola 2002, Colgan & Pindzola 2003, Horner *et al* 2004). These DPI amplitudes are matched by their (e,2e) counterparts derived from TDCS (3) which is calculated by using the same techniques. In the homo-shell atoms, the choice of the ionic state in the (e,2e) reaction is obvious (He^+ $1s$ and Be^+ $2s$). In hetero-shell atoms, we notice that it is the inner K-shell that is more readily photoionized in the DPI process in order to facilitate exchange of the recoil momentum with the nucleus. Therefore, it is the outer L-shell that is knocked out to produce the secondary photoelectron.

In Figure 1 we show symmetric DPI amplitudes for the ground state helium $1s^2\ ^1S$, the metastable helium $1s2s\ ^1S$, the ground state lithium $1s^22s\ ^2S$ and beryllium $2s^2\ ^1S$ (from top to bottom). All the amplitudes are calculated at the equal energy sharing of $E_1 = E_2 = 10$ eV. Both the DPI and (e,2e) amplitudes have the folding symmetry relative to the midpoint at $\theta_{12} = \pi$. We use this symmetry to accommodate the amplitudes of two different processes on the same plot. The DPI amplitudes are displayed on the left half of each panel while their (e,2e) counterparts for the He^+ $1s$, He^+ $2s$, Li^+ $1s2s\,^1S$ and Be^+ $2s$ ions, respectively, are exhibited on the corresponding right half.

When inspecting Figure 1, we encounter immediately the two striking features. First, we observe a very close similarity between the DPI amplitude and the corresponding dipole singlet (e,2e) amplitude for all three targets. This observation

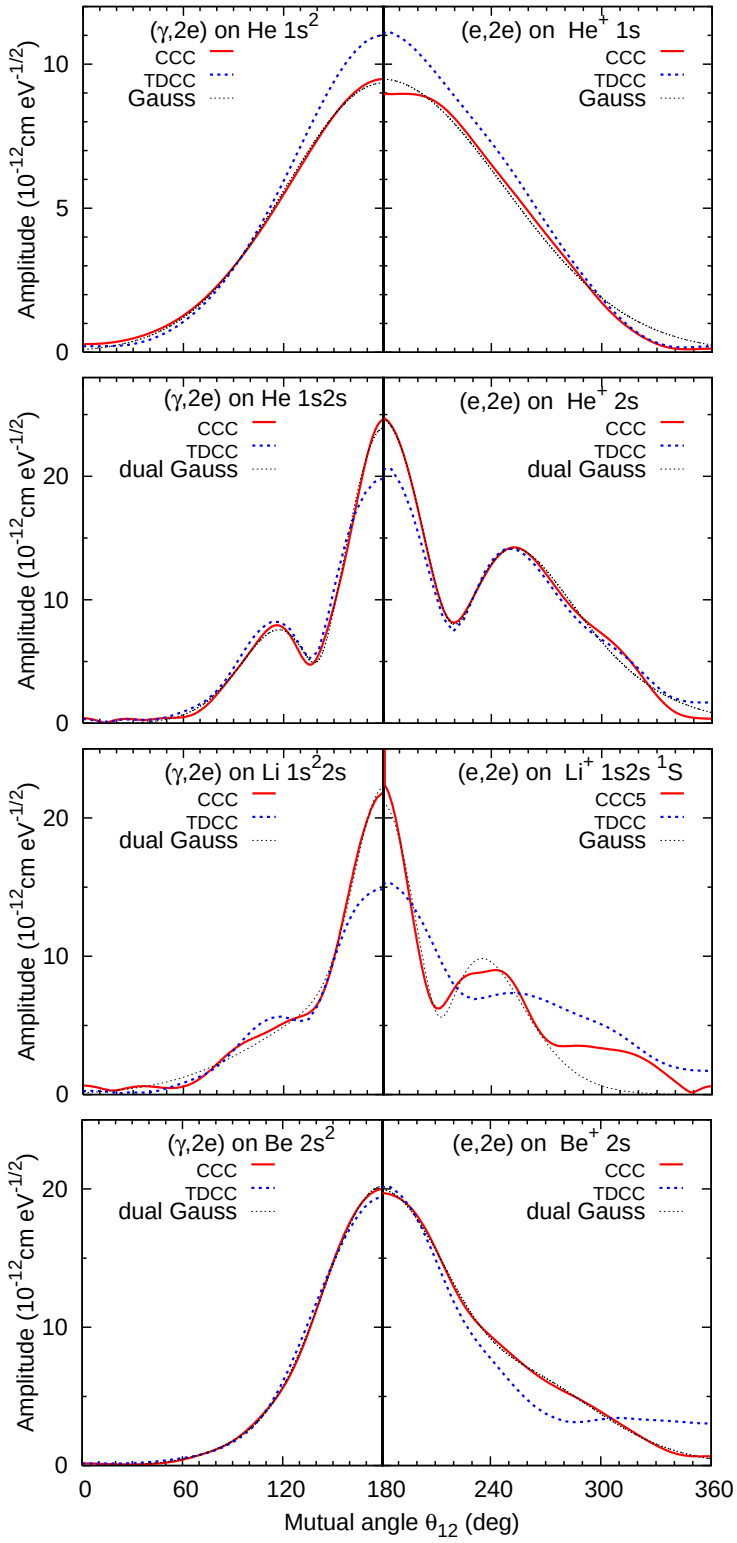

Figure 1. (Color online)
Left panels show the moduli of symmetric DPI amplitudes $|\mathcal{M}^g(\theta_{12})|$ for He $1s^2\ ^1S$, He* $1s2s\ ^1S$, Li $1s^22s$ and Be $2s^2\ ^1S$ (from top to bottom) at the equal energy sharing of $E_1 = E_2 = 10$ eV. The right panels display the moduli of symmetric dipole singlet (e,2e) amplitudes $|\mathcal{M}^g_{(e,2e)}(\theta_{12})|$ of the corresponding singly charged ions He^+ $1s$, He^+ $2s$, Li^+ $1s2s\ ^1S$ and Be^+ $1s^22s$. The (e,2e) amplitudes are scaled to their $(\gamma, 2e)$ counterparts. The CCC calculations are displayed with the red solid lines, the TDCC calculations are shown with the blue dotted lines. The Gaussian parameterizations (2) (top panel) and (4) (other panels) of the CCC results are visualized with the thin dotted lines.

supports our hypothesis that the angular correlation pattern in DPI is formed via inter-electron interaction in the final doubly ionized state which is identical in the (γ,2e) reactions and the dipole singlet (e,2e) reactions. This also indicates that the ground state correlation in the neutral atom, which is present in (γ,2e) but absent in (e,2e), is largely irrelevant to this pattern, contrary to the claim made by Citrini *et al* (2003).

The second striking feature visible in Figure 1 is a prominent double-peak structure of the (γ,2e) and (e,2e) amplitudes in the case of the metastable helium and the ground state lithium. While the amplitudes of the ground state He on the top panel of Figure 1 can be fitted accurately with the standard Gaussian ansatz (2), a more general dual Gaussian parameterization is required in the case of Li and metastable He:

$$G(t) = A_1 \exp\left[-2\ln 2\left(\frac{\pi-\theta_{12}}{\Delta\theta_1}\right)^2 \right] + e^{i\phi} A_2 \exp\left[-2\ln 2\left(\frac{\pi-\theta_{12}}{\Delta\theta_2}\right)^2 \right]. \quad (4)$$

The complex phase factor represents the interference of the two Gaussians. The five constants $A_{1.2}$, $\Delta\theta_{1,2}$ and ϕ are used as fitting parameters. Thus obtained dual Gaussian parameterization is shown on the panels 2-4 (from top to bottom) for both the (γ,2e) and (e,2e) amplitudes calculated with the CCC model. The raw amplitude and its dual Gaussian representation can hardly be distinguished in the figure. Some minor deviation is only discernible for the (e,2e) amplitude at a nearly parallel escape of the two continuum electrons. The need to use the dual Gaussian parameterization (4) is less obvious in the case of Be but it certainly provides a much better fit to the CCC (e,2e) amplitude.

To gain more insight into the origin of such a profound difference between the amplitudes of the three atomic targets shown in Figure 1, we focus our attention on the much more transparent (e,2e) reaction which is not affected by the ground state correlation in the neutral atom. In Figure 2 we display the (e,2e) amplitudes for the He^+ $1s$ (left) and He^+ $2s$ (right) ions across a wider range of energies. The five rows of panels, from top to bottom, correspond to the total energy of the scattering system fixed at 40, 20, 10, 4 and 1 eV and shared equally between the two outgoing electrons. The TDCC calculations are displayed in the figure. As in Figure 1, we fit the amplitudes for the He^+ $1s$ ion with the standard Gaussian ansatz (2) while the dual Gaussian parameterization (4) is applied to the He^+ $2s$ amplitude.

The Gaussian width parameter of the He^+ $1s$ amplitude increases gradually with the energy of the scattering system. It changes continuously from $\Delta\theta = 87°$ at 1 eV (bottom) to 119° at 40 eV (top). This is in line with Wannier threshold theory (Wannier 1953) which predicts the vanishing Gaussian width when the total energy of the scattering system tends to zero.

The larger of the two width parameters of the dual Gaussian parameterization for the He^+ $2s$ amplitude has a very similar energy dependence. This may be observed as the widening of the background of the $2s$ amplitude with the energy increase. However, its central part is formed by interference with the second Gaussian of a considerably smaller width which varies insignificantly around 60°. The ratio of the magnitude factors of the narrow and wide Gaussians is nearly constant at about ~ 1.5 while the phase shift

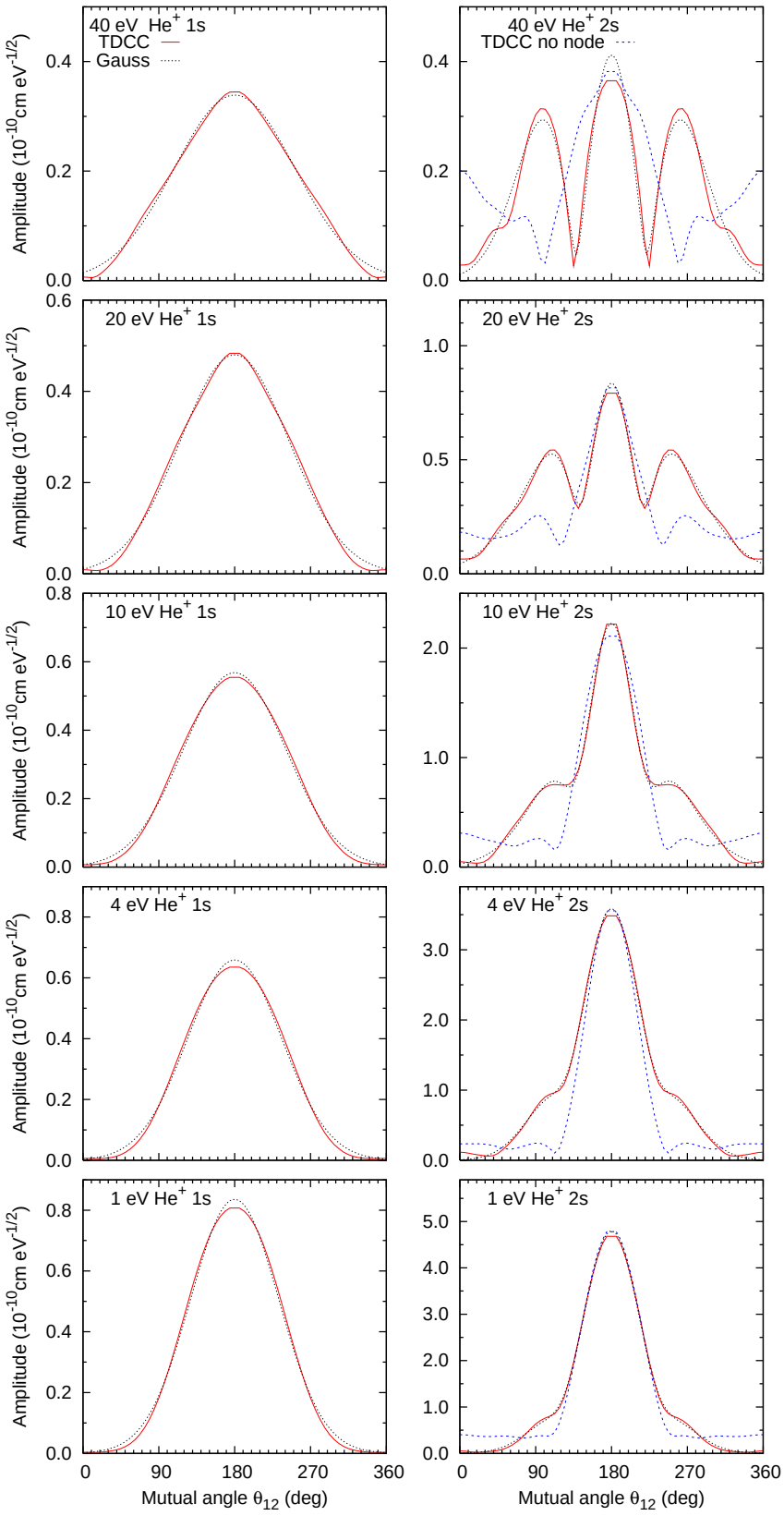

Figure 2. (Color online) The moduli of the dipole singlet amplitudes $|\mathcal{M}^g_{(e,2e)}(\theta_{12})|$ of the He^+ $1s$ (left) and He^+ $2s$ (right) ions. The total energy of the scattering system varies from 40 eV (top) to 1 eV (bottom). The raw amplitudes (TDCC - red solid line) are fitted with the Gaussian ansatz (He^+ $1s$) and the dual Gaussian ansatz (He^+ $2s$) (black thin dotted line). The TDCC amplitude for He^+ $\overline{2s}$ is shown with blue dashed line.

between the two Gaussians is increasing gradually with energy from 145° to nearly 180°. This phase shift increase changes dramatically the nature of the interference between the two Gaussians across the studied collision energy range. Indeed, at the lowest collision energy of 1 eV, the two channels interfere constructively and the resulting $2s$ amplitude is more than 5 times larger than its $1s$ counterpart. Conversely, at the top collision energy of 40 eV, there is a very strong destructive interference and the $2s$ and $1s$ amplitudes are about the same height.

The interference pattern is qualitatively similar for the Be^+ $2s$ amplitudes which are exhibited in Figure 3. However, in the case of Be^+, the phase shift is somewhat smaller varying from 140° to 170°. Thus, the onset of a strong destructive interference is shifted towards larger energies. It is manifested most profoundly for the largest excess energy of 40 eV.

As we argued in the introduction, the Gaussian width may be linked to the radial extent of the target orbital bound to the singly charged ion. A more sparse target orbital can be reached by a larger number of partial waves of the continuous electron which leads to a narrower Gaussian. Thus, it would be natural to associate the two distinct Gaussians, the wide and narrow, with two characteristic areas in the target coordinate space. In principle, the mixture of the two collision channels $e^- + A^+(1s)$ and $e^- + A^+(2s)$ in the close-coupling expansion may be responsible for the observed interference pattern. However, we must rule out this scenario. Indeed, the $e^- + A^+(1s)$ channel is closed in the case of Be^+ at the incident energies below the K edge which are considered here. In addition, we have explicitly verified that removal of the $1s$ channel from the CCC expansion does not change the He^+ $2s$ amplitude in any appreciable way.

We also have to mention that the energy scale of the (e,2e) reaction on the He^+ ion is given by the corresponding ionization potential which is 4 times larger for the $1s$ state than the $2s$ state. Therefore the same collision energy takes the He^+ $2s$ ion 4 times farther away from the threshold in comparison with the He^+ $1s$ ion. This could, in principle, lead to a larger deviation from the Wannier threshold theory and the standard Gaussian ansatz for the He^+ $2s$ ion state. However, this deviation is already clearly seen at the lowest scattering energy of 1 eV considered in the present work. At the same time, the He^+ $1s$ amplitude is perfectly Gaussian at the respective energy of 4 eV.

It is also worth mentioning that the two complex phase shifted terms of the DPI amplitude were introduced earlier by Krässig *et al* (1996) to describe DPI leading to various $np^4\ ^{2S+1}L$ final states of noble gas atoms. This phase shift, however, was due to interference of the s- and d-partial waves emitted from the np^6 target electron shell. This phase shift is not relevant to the present case of s-shell ionization.

In the view of the above arguments, we have come up with the following explanation of the observed interference phenomena. When we examine the He^+ radial wave functions shown in Figure 4, we see that the $2s$ orbital has two distinct peaks. The peak of the positive oscillation has a radial extent which is very similar to that of the $1s$ orbital. The latter is scaled in the figure to $2s$ for better clarity. The negative oscillation of the $2s$ orbital has a significantly larger radial extent. We suggest that these two peaks of the

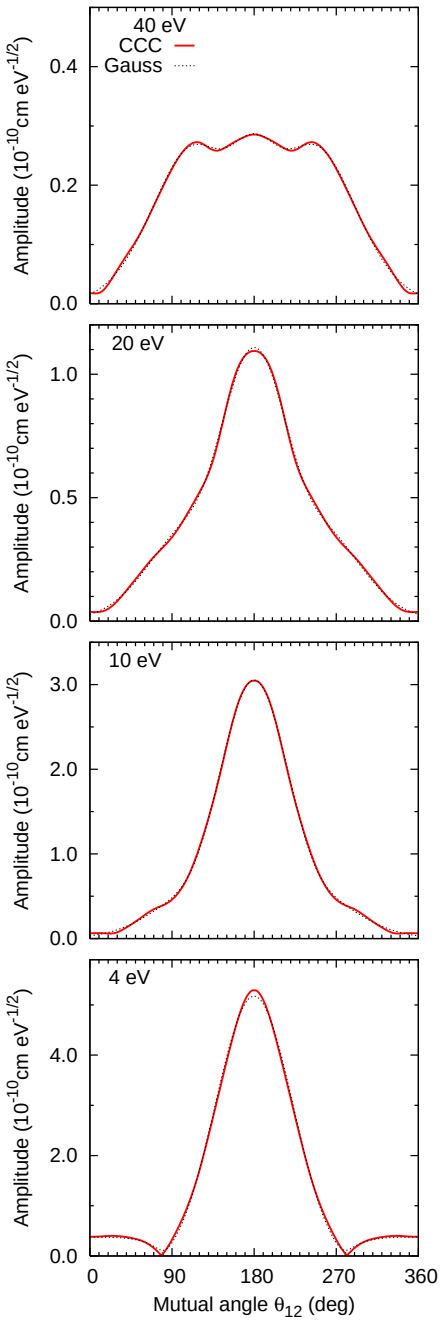

Figure 3. (Color online) The moduli of the dipole singlet amplitudes $|\mathcal{M}^g_{(e,2e)}(\theta_{12})|$ of the Be^+ $1s^2 2s$ ion. The total energy of the scattering system varies from 40 eV (top) to 4 eV (bottom). The raw amplitudes (CCC - red solid line) are fitted with the dual Gaussian ansatz (black thin dotted line).

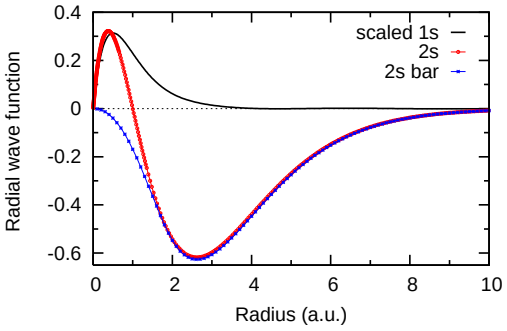

Figure 4. (Color online) Radial wave functions $P_{1s}(r)$ (scaled to $2s$), $P_{2s}(r)$ and $P_{\overline{2s}}(r)$ of the He^+ ion.

target electron density each produce their own Gaussians with the wider and narrower width. This explains why the ratio of the magnitude factors of the two Gaussians is nearly constant. The opposite signs of the half-cycles also explains why the phase shift between the Gaussians tends to 180°. At lower scattering energies, the phase shift is distorted by dispersion of the partial waves with various ℓ. With the energy increase, the partial wave phases tend to converge with ℓ as $\sigma_\ell(k) = \arg\Gamma\left(1+\ell-iZ_{\rm eff}/k\right)$, where k is the momentum of the ejected electron. Partial wave dispersion is stronger in Be^+ and hence the Gaussian phase parameter tends to 180° at large collision energies.

To test this hypothesis, we performed an additional set of TDCC calculations with a nodeless $\overline{2s}$ pseudo-orbital which is also shown in Figure 4. This $\overline{2s}$ pseudo-orbital is very similar to the real $2s$ orbital apart from the inner region for $r < 1.5$ a.u. Thus constructed the He^+ $\overline{2s}$ amplitudes are shown on the corresponding panels of Figure 2. As compared to the physical He^+ $2s$ amplitudes, they show significantly reduced interference fringes, especially at low scattering energies. The unphysical He^+ $\overline{2s}$ amplitude does not vanish at the parallel emission which we presume is an artefact of this model.

We also analyzed the (e,2e) amplitudes for the He^+ $3s$ and Be^+ $3s$ ions. Even though we did observe some interference fringes across the studied energy range, they are significantly weaker than in the case of the $2s$ amplitudes. This may be explained by interplay of the three oscillations of alternate sign.

Modern experimental techniques allow for direct DPI amplitude measurements (Bolognesi *et al* 2003, Knapp *et al* 2005). Therefore, the theoretically predicted amplitude interference effects can be detected experimentally. These effects are so profound that they leave a clear signature in the photoelectron angular distribution. On the two top panels of Figure 5 we show the angular correlation pattern for two equal energy photoelectrons $E_1 = E_2 = 10$ eV emitted in the process of DPI of the ground $1s^2$ state (left) and the metastable $1s2s\,^1S$ state (right) of the helium atom. In our illustration, we consider the coplanar geometry in which both electrons are emitted in the polarization plane of light. The interference effects are clearly seen in the case of

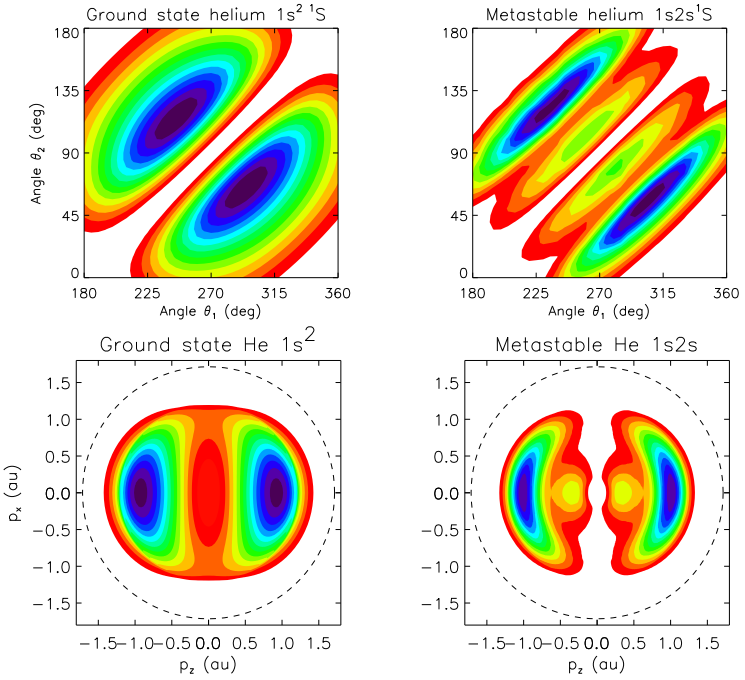

Figure 5. (Color online) Top row: TDCS of DPI of the ground $1s^2\,{}^1S$ state (left) and the metastable $1s2s\,{}^1S$ state (right) of He at the symmetric coplanar geometry with $E_1 = E_2 = 10$ eV. The photoelectron angles θ_1, θ_2 are counted from the polarization axis of light. Bottom row: the recoil ion momentum distribution of the same targets at the excess energy of 20 eV.

the metastable He with significantly narrowing and doubling the major features which correspond to the mutual angle of photoelectrons of about $\sim 120°$.

The interference effects in metastable He are so strong that they survive partial integration over various energy sharing's and mutual angles and manifest themselves clearly in the recoil ion momentum distribution. In a typical cold target recoil ion momentum spectroscopy COLTRIMS experiments (Bräuning *et al* 1997, Zhu *et al* 2009), the recoil momentum distribution is projected onto the polarization plane (x, z) by integration over the y-component of the momentum. Such distributions are displayed on the two bottom panels of Figure 4 for the ground $1s^2\,{}^1S$ state (left) and the metastable $1s2s\,{}^1S$ state (right) of the helium atom at the excess energy of 20 eV. This energy corresponds to the maximum recoil momentum $p_{\max} = 1.7$ a.u. which is indicated in the figure by a dashed circle.

In conclusion, we identify and interpret interference effects in double photoionization (DPI) of L-shell atomic targets. Not far away from the DPI threshold, where the knock-out mechanism is dominant, these interference effects can be traced to the electron impact ionization of the corresponding singly charged ion. The dipole singlet amplitude of the doubly symmetric (e,2e) reaction on the He^+ $2s$, Li^+ $1s2s$ and Be^+ $2s$ ions can be parametrized using the dual Gaussian ansatz. The two Gaussian width parameters differ significantly. We argue that the wider Gaussian can be attributed to

the inner region of the target coordinate space whereas the narrow Gaussian originates from the outer region. We validate this hypothesis by considering the electron impact ionization of the nodeless $\overline{2s}$ orbital in which the inner region is significantly depleted. The corresponding amplitude has the wider Gaussian largely removed. We propose several measuring schemes to observe these interference effects experimentally.

Acknowledgments

We thank Tim Reddish and Alain Huetz for critical reading of the manuscript. The Los Alamos National Laboratory is operated by Los Alamos National Security, LLC for the National Nuclear Security Administration of the U.S. Department of Energy under Contract No. DE-AC5206NA25396. A portion of this work was performed through DOE and NSF grants to Auburn University. The computational work was carried out at the National Institute for Computational Sciences in Oak Ridge, TN. Resources of the Australian National Computational Infrastructure (NCI) Facility and its Western Australian node iVEC are gratefully acknowledged.

Bolognesi P, Kheifets A S, Bray I, Malegat L, Selles P, Kazansky A K & Avaldi L 2003 A procedure to extract the complex amplitudes of He photodouble ionization from experimental data *J. Phys. B* **36**(16), L241

Bräuning H, Dörner R, Cocke C L, Prior M H, Krässig B, Bräuning-Demian A, Carnes K, Dreuil S, Mergel V, Richard P, Ullrich J & Schmidt-Böcking H 1997 Recoil ion and electronic angular asymmetry parameters for photo double ionization of helium at 99 eV *J. Phys. B* **30**(19), L649–L655

Citrini F, Malegat L, Selles P & Kazansky A K 2003 Direct double photoionization of the valence shell of Be *Phys. Rev. A* **67**, 042709

Colgan J & Pindzola M S 2002 Double photoionization of beryllium *Phys. Rev. A* **65**(2), 022709

Colgan J & Pindzola M S 2003 Total and differential cross-section calculations for the double photoionization of the helium $1s2s\,^{1,3}S$ states *Phys. Rev. A* **67**(1), 012711

Horner D A, Colgan J, Martín F, McCurdy C W, Pindzola M S & Rescigno T N 2004 Symmetrized complex amplitudes for He double photoionization from the time-dependent close-coupling and exterior complex scaling methods *Phys. Rev. A* **70**(6), 064701

Huetz A, Selles P, Waymel D & Mazeau J 1991 Wannier theory for double photoionization of noble gases *J. Phys. B* **24**(8), 1917

Kheifets A 2001 On different mechanisms of the two-electron atomic photoionization *J. Phys. B* **34**(8), L247

Kheifets A S, Fursa D V, Bray I, Colgan J & Pindzola M S 2010 Differential cross sections of double photoionization of lithium *Phys. Rev. A* **82**(2), 023403

Kheifets A S, Fursa D V, Hines C W, Bray I, Colgan J & Pindzola M S 2010*a* Spin effects in double photoionization of lithium *Phys. Rev. A* **81**(2), 023418

Kheifets A S & Bray I 2000 Equal energy-sharing double photoionization of helium from near-threshold to high energies *Phys. Rev. A* **62**(6), 065402

Kheifets A S & Bray I 2001 Frozen-core model of the double photoionization of beryllium *Phys. Rev. A* **65**(1), 012710

Kheifets A S & Bray I 2002 Symmetrized amplitudes of the helium-atom double photoionization *Phys. Rev. A* **65**(2), 022708

Kheifets A S & Bray I 2006 Angular correlation in the two-electron continuum *Phys. Rev. A* **73**(2), 020708

Knapp A, Krässig B, Kheifets A, Bray I, Weber T, Landers A L, Schössler S, Jahnke T, Nickles J, Kammer S, Jagutzki O, Schmidt L P H, Schöffler M, Osipov T, Prior M H, Schmidt-Böcking H, Cocke C L & Dörner R 2005 Photo double ionization of helium 100 eV and 450 eV above threshold: III. Gerade and ungerade amplitudes and their relative phases *J. Phys. B* **38**(6), 645

Krässig B, Schaphorst S J, Schwarzkopf O, Scherer N & Schmidt V 1996 State dependence of $np^4\ ^{2S+1}l$ angular correlation patterns in double photoionization *J. Phys. B* **29**(18), 4255

Schwarzkopf O, Krässig B, Elmiger J & Schmidt V 1993 Energy- and angle-resolved double photoionization in helium *Phys. Rev. Lett.* **70**(20), 3008–3011

Wannier G H 1953 Treshold ionization by electron impact ... *Phys. Rev.* **90**, 817–825

Zhu G, Schuricke M, Steinmann J, Albrecht J, Ullrich J, Ben-Itzhak I, Zouros T J M, Colgan J, Pindzola M S & Dorn A 2009 Controlling two-electron threshold dynamics in double photoionization of lithium by initial-state preparation *Phys. Rev. Lett.* **103**(10), 103008